Coupling of a Jahn–Teller pseudorotation with a hindered internal rotation in an isolated molecule: 9-hydroxytriptycene

Alan Furlan, Samuel Leutwyler, and Mark J. Riley

Citation: The Journal of Chemical Physics **109**, 10767 (1998); doi: 10.1063/1.477775
View online: http://dx.doi.org/10.1063/1.477775
View Table of Contents: http://scitation.aip.org/content/aip/journal/jcp/109/24?ver=pdfcov
Published by the AIP Publishing

Coupling of a Jahn–Teller pseudorotation with a hindered internal rotation in an isolated molecule: 9-hydroxytriptycene

Alan Furlan
Physikalisch-Chemische Institut, Universität Zürich, Winterthurerstrasse 190, CH-8057 Zürich, Switzerland

Samuel Leutwyler
Departement für Chemie und Biochemie, Universität Bern, Freiestrasse 3, CH-3000 Bern 9, Switzerland

Mark J. Riley[a)]
Department of Chemistry, University of Queensland, St Lucia, 4072, Australia

(Received 29 July 1998; accepted 17 September 1998)

The irregular vibronic structure in the $S_1 \leftarrow S_0$ resonant two-photon ionization (R2PI) spectrum of supersonically cooled triptycene is a result of a classic $E \otimes e$ Jahn–Teller effect [A. Furlan *et al.*, J. Chem. Phys. **96**, 7306 (1992)]. This is well characterized and can be used as an effective probe of intramolecular perturbations. Here we examine the $S_1 \leftarrow S_0$ R2PI spectrum of 9-hydroxytriptycene and the fluorescence from various excited state vibronic levels. In this system the pseudorotation of the Jahn–Teller vibration is strongly coupled to the torsional motion of the bridgehead hydroxy group. This torsional motion results in a tunneling splitting in both the ground and excited states. The population of the upper level in the ground electronic state results in additional vibronic transitions becoming symmetry allowed in the R2PI spectrum that are forbidden in the bare triptycene molecule. The assignment of the R2PI and fluorescence spectra allows the potential energy surfaces of these vibrational modes to be accurately quantified. The full C_{3v} vibronic point group must be used to interpret the spectra. The time scale of the internal rotation of the–OH group and the butterfly flapping of the Jahn–Teller pseudorotation are of similar magnitude. The tunneling between the nine minima on the three dimensional potential energy surface is such that the Jahn–Teller pseudorotation occurs *in concert* with the–OH internal rotation. The Berry phase that is acquired during this motion is discussed. The simple physical picture emerges of the angle between two of the three benzene moieties opening in three equivalent ways in the S_1 electronic state. This geometry follows the position of the hydroxy group, which preferentially orients itself to point between these two rings. © *1998 American Institute of Physics.* [S0021-9606(98)02348-4]

I. INTRODUCTION

We recently described the resonant two-photon ionization (R2PI) spectra of triptycene (1,9-dihydro-9, 10[1′,2′]benzenoanthracene).[1] The complicated and irregular vibronic structure in the $S_1 \leftarrow S_0$ transition could be almost completely assigned in terms of a simple $E' \otimes e'$ Jahn–Teller system. In addition, the same parameters of the $E' \otimes e'$ vibronic Hamiltonian could be used to quantitatively reproduce the observed fluorescence emission spectra from some 13 vibronic levels.[1] The dynamical Jahn–Teller effect has been described some time ago, but clear and unambiguous spectroscopic examples of resolved vibronic structure in isolated molecules have been lacking until recently.[1–7]

The triptycene molecule can be thought of as a covalently bound trimer of benzene moieties fixed at 120° to each other by two bridgehead C–H groups. The Jahn–Teller active e' vibration has been identified[2] as the low frequency mode shown in Fig. 1. The e'_x component of this vibration could be described as a flapping, or butterfly motion, of the molecule. The resulting $E \otimes e$ Jahn–Teller surface of the S_1 excited electronic state has three minima, each corresponding to geometry of triptycene where there is a large angle change between two of the benzene rings.[3] While it is not possible to determine whether this geometry change corresponds to a opening or closing of two benzene rings from the equilibrium value of 120°; it has previously been assumed that the three minima correspond to a geometry where this angle has decreased. However, the present work implies that the minima actually correspond to a geometry of the opposite sign, where the angle between two benzene rings has *increased*. In the triptycene molecule, the calculated tunneling splitting of 0.93 cm^{-1} indicates that the above large geometry change occurs with a period of 36 ps.

Subsequently this molecule has been used as a test bed to study both higher-order terms and perturbations to $E \otimes e$ type Jahn–Teller systems. For example, we have studied the vibronic Hamiltonians of trimers in general,[4,5] the participation of a_2 vibrations via momentum coupling,[5,6] chemical substitution,[7] and the formation of van der Waals complexes.[3]

The successful interpretation of the triptycene spectra is partially due to the molecule itself, as the molecular vibrations clearly divide into low and high frequency groups.[2] The normal coordinates of the eight lowest energy vibrations can be generated by the symmetry adapted linear combinations

a)Electronic mail: riley@chemistry.uq.edu.au

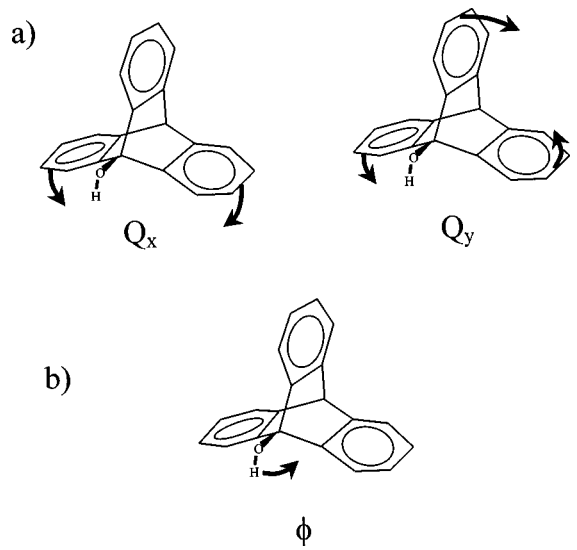

FIG. 1. Low frequency vibrations in 9-hydroxytriptycene. (a) The normal coordinates of the two components of the Jahn–Teller active *e* vibration; and (b) the hindered rotational motion, ϕ, of the hydroxy group.

of the translations and rotation of three rigid benzene molecules.[2] All vibrations containing internal benzene motions are much higher in energy. The active flapping e' mode at 64 cm^{-1}, is by far the lowest energy vibration. It also exhibits the strongest coupling to the first excited state, accounting for over ~98% of the intensity in the R2PI and fluorescence spectra. This low frequency and strong coupling result in very long progressions of up to 35 members in the fluorescence emission.[1] A careful examination of the fluorescence spectra reveals the participation of five other $(a_1', a_2', 3e')$ vibrations, however the intensity from the 64 cm^{-1} e' vibration dominates.

One way to perturb this $E \otimes e$ Jahn–Teller system on a time-scale commensurate with the tunneling between the Jahn–Teller minima is to add a group that undergoes hindered internal rotation with a tunneling rate of its own. This situation is realized for 9-hydroxytriptycene, see Fig. 1. The terminal hydroxy group, attached to one of the bridgehead carbon atoms, undergoes a low frequency tunneling motion across potential energy barriers that are clearly sensitive to the change of the benzene angles from 120°. In addition, while the point group of this nonrigid molecule will be reduced from D_{3h} to C_{3v}, this does not affect the $E \otimes e$ Jahn–Teller problem. The vibronic group (isomorphous with the C_{3v} point group and the G_6^2 group for non-rigid molecules) remains the same. Here we will use *A*, *B*, and *E* labels for the irreducible representations of the C_{3v} point group rather than the usual A_1, A_2, and *E* labels to avoid confusion with the first- and second-order Jahn–Teller coupling constants which are also labeled A_1 and A_2.

II. EXPERIMENTAL METHODS AND RESULTS

Resonant two-photon ionization (R2PI) spectra of 9-hydroxytriptycene in a pulsed supersonic jet were obtained with the apparatus that has been described in detail elsewhere.[8] 9-hydroxytriptycene (TOH) was prepared by the procedure given in Ref. 9, and purified by recrystallization in methanol. The pale yellow crystals with a melting point of ~245° C were placed inside the nozzle and heated to 140° C. The carrier gas was Ne at a backing pressure of 1.1 bar. Complexation of the chromophore with Ne, which has been discussed in detail elsewhere,[3] is very weak at the expansion conditions used for this study. The R2PI spectra were recorded in the range of 272–276 nm, with the tunable laser pulses provided by the frequency-doubled output of a Nd: yttrium–aluminium–garnet (YAG)-pumped dye laser. The laser beam with pulse energies of ~3 μJ/pulse was slightly expanded to avoid saturation of the $S_0 \leftarrow S_1$ transition.

The R2PI $S_1 \leftarrow S_0$ spectrum of TOH is shown in Fig. 2a, relative to the electronic origin at 36 333.4 cm^{-1}. This spectrum only contains bands attributed to the ^{12}C, ^{1}H isotopomer of free TOH and not to any van der Waals complexes. There are rough similarities between this spectrum and that of plain triptycene.[1] The most obvious difference is the doubling of the vibronic bands, each main band has another ~2.6 cm^{-1} to lower energy. In addition there appears a triplet of bands labeled **e** at ~110 cm^{-1} above the origin, while the band **c** in triptycene is very weak in TOH. The vibronic bands are labeled **a**, **b**, **c** ... in analogy with the labels given to triptycene,[1] and correspond to very similar vibronic states until the new band **e** in TOH. Above ~150 cm^{-1} this correspondence breaks down.

The doubling of the main lines of the triptycene spectrum can be attributed to ''hot bands'' from the population of the low lying vibrational *E* level associated with the –OH torsional hindered rotation in the ground electronic state. We make this assignment for a number of reasons. The experimental conditions can be varied so that there is a higher population of the excited *E* level in the ground electronic state. This results in an observed increase in the intensity of the lower energy band of the pairs that appear in the R2PI spectrum. To test this assignment of the doublets, R2PI measurements with deuterated triptycene were also performed. The R2PI spectrum of TOH with the hydroxy group partially deuterated shows doublets with a smaller splitting as the reduced mass of the hindered rotation decreases. Selection rules dictate that the 2.6 cm^{-1} splitting actually corresponds to a *difference* in the ground and excited state splittings. However, it will be shown that the excited state splitting is very small and the 2.6 cm^{-1} splitting is approximately equal to the ground state splitting.

Dispersed fluorescence measurements were carried out by exciting the molecular beam 8 mm in front of the nozzle and collecting the fluorescence with a quartz lens and dispersing it with a 1.0 m monochromator. The monochromator slit width was varied depending on the fluorescence intensity of the excited S_1 level. The resulting bandpass was 5–10 cm^{-1} [full width at half maximum (FWHM)]. All spectra are corrected for laser power fluctuations and background.

The emission spectra shown in Figs. 3 and 4 consist predominantly of one progression, with different Franck–Condon envelopes depending on which vibronic level is excited. This progression is very harmonic with a ground state vibrational frequency of 63.6 cm^{-1}, and extends to more than 20 members in some cases. The emission spectra were not used in fitting the vibronic Hamiltonian. However, their

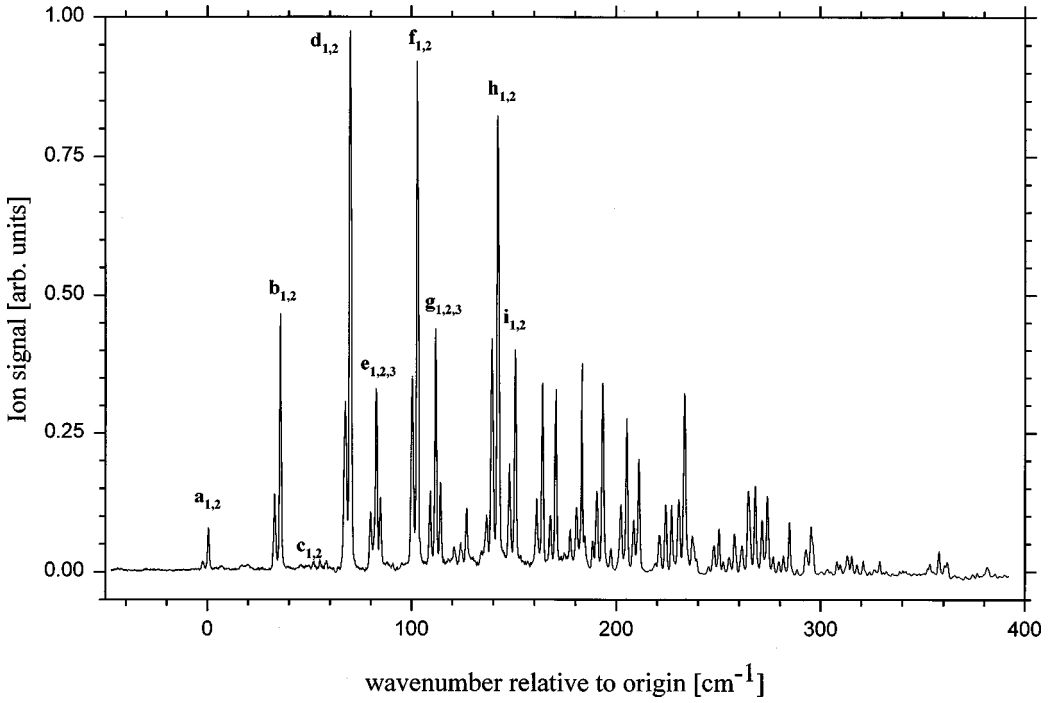

FIG. 2. The R2PI spectrum of 9-hydroxytriptycene relative to the $S_1 \leftarrow S_0$ electronic origin at 36 333.4 cm^{-1}. The vibronic bands labels **a** to **h** are referred to in the text. The subscripts 1 and 2 denote hot and cold bands, respectively.

nodal pattern provides the key to understanding the R2PI spectrum. Qualitatively, the minima in the envelope of the emission spectra reveal the nodes in the radial direction of the excited state $E \otimes e$ vibronic wave functions. The emission from levels **a**, **b**, and **d** shown in Fig. 3 can be given the approximate radial quantum numbers 0, 1, and 2, respectively, in analogy to the assignments found for triptycene.[1] Levels $\mathbf{e_1} - \mathbf{e_3}$ (Fig. 4), which are absent in the R2PI spectrum of triptycene, exhibit no nodes in the emission spectra. The assignment of these levels will be further discussed in Sec. IV.

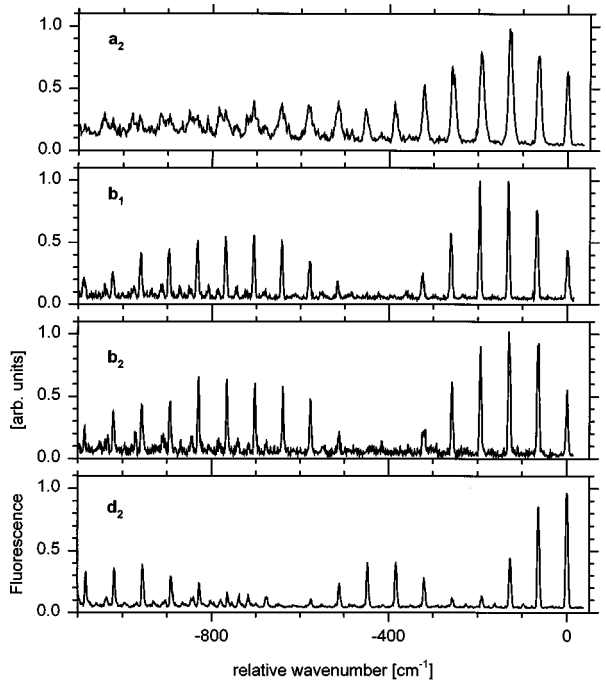

FIG. 3. The single vibronic level fluorescence emission spectra of TOH excited to levels $\mathbf{a_2}$, $\mathbf{b_1}$, $\mathbf{b_2}$, and $\mathbf{d_2}$. The abscissa is relative to the excitation energy.

III. COMPUTATIONAL METHODS

A. The vibronic Hamiltonian

We have used the basic $E \otimes e$ Jahn–Teller vibronic Hamiltonian that has proved successful in interpreting the

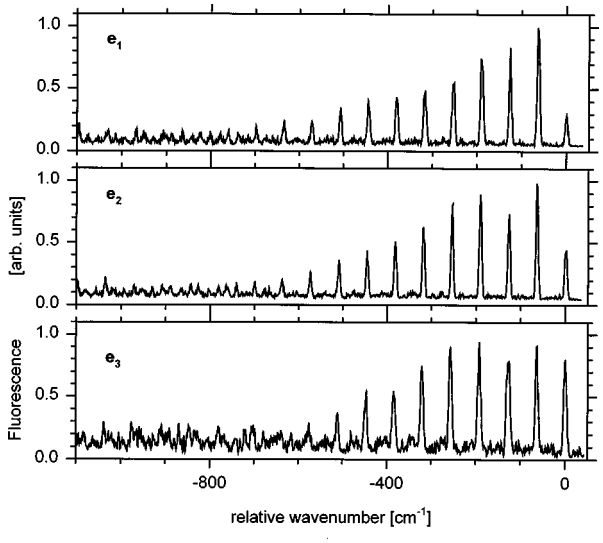

FIG. 4. The single vibronic level fluorescence emission spectra of TOH excited to levels $\mathbf{e_1}$, $\mathbf{e_2}$, and $\mathbf{e_3}$. The abscissa is relative to the excitation energy.

spectrum of triptycene[1] and have included the torsional coordinate, ϕ, of the hydroxy group in what we will call a $E\otimes(e+\phi)$ coupling scheme. Clearly the hindered rotation of the hydroxy group [Fig. 1b] will interact with the Jahn–Teller e mode as the barrier to the hindered rotation changes as a function of the angle between the benzene rings [Fig. 1a].

The $E\otimes(e+\phi)$ vibronic Hamiltonian is given by

$$\mathbf{H_{VIB}}=\mathbf{H_0}+\mathbf{H_{JT}}+\mathbf{H_{JT\phi}},$$

$$\mathbf{H_0}=\frac{1}{2}\left[-h\nu\left(\frac{\partial^2}{\partial X^2}+\frac{\partial^2}{\partial Y^2}\right)+K_2(X^2+Y^2)\right]\mathbf{I}+\left[-B\frac{\partial^2}{\partial\phi^2}+1/2V_3(1-\cos 3\phi)\right]\mathbf{I},$$

$$\mathbf{H_{JT}}=A_1[-X\sigma_z+Y\sigma_x]+A_2[-(X^2-Y^2)\sigma_z+2XY\sigma_x], \quad (1)$$

$$\mathbf{H_{JT\phi}}=B_1[X\cos\phi+Y\sin\phi]I,$$

$$\mathbf{I}=\begin{pmatrix}1&0\\0&1\end{pmatrix},\quad \sigma_x=\begin{pmatrix}0&1\\1&0\end{pmatrix},\quad \sigma_z=\begin{pmatrix}-1&0\\0&1\end{pmatrix}.$$

Here the $\mathbf{H_0}$ contains the vibrational Hamiltonians of the harmonic Jahn–Teller e mode and the hindered rotation of the ϕ coordinate. The X and Y are the dimensionless coordinates of the e_x and e_y vibrational modes. The use of dimensionless coordinates allows the parameters to be expressed in energy units. It is convenient to express X and Y in polar coordinates ρ, θ in following sections. These radial and angular coordinates are given by $\rho=[X^2+Y^2]^{1/2}$, $\theta=\tan^{-1}[Y/X]$. The Jahn–Teller angular coordinate θ should not be confused with the hindered internal rotation coordinate ϕ.

$\mathbf{H_{JT}}$ contains the Jahn–Teller coupling terms and $\mathbf{H_{JT\phi}}$ contains the coupling between the Jahn–Teller and ϕ modes. The analogous ground state vibronic Hamiltonian is given by $\mathbf{H_0}+\mathbf{H_{JT\phi}}$ without the matrix $\mathbf{I}$ and setting $K_2=h\nu$. It will be shown that it is important to include the coupling between the Jahn–Teller mode and the internal rotation in the ground electronic state even though it is nondegenerate and Jahn–Teller inactive. In the excited state $h\nu$ is the same as in the ground state and K_2 is allowed to be different. We allow the excited state to have a different vibrational frequency for the e vibration, as this was found to be important in the interpretation of the triptycene spectrum.[1] The final parameters are then adjusted so the terms in $\mathbf{H_0}$ are harmonic ($K_2=h\nu$) by ''scaling'' the coordinates. We use this method so that the excited state basis can be expressed in terms of the ground state e basis, simplifying the calculation of the spectrum.[1]

The vibronic basis functions Ψ consist of a quadruple product of one electronic, ψ, and three vibrational, ϕ, states.

$$\Psi=\sum_{\ell=x,y}\sum_{i+j=0}^{n_e}\sum_{k=-n_\phi}^{+n_\phi}a_{lijk}\psi_l\phi_i\phi_j\phi_k. \quad (2)$$

The electronic states, ψ_x and ψ_y are the two components of the E excited S_1 state; ϕ_i and ϕ_j are the one-dimensional harmonic oscillator basis functions of the e vibration, and ϕ_k are the trigonometric functions for the torsional coordinate.

$$\begin{aligned}\phi_k&=\sqrt{1/\pi}\,\sin(|k|\phi) \quad k<0\\&=\sqrt{1/2\pi} \quad k=0\\&=\sqrt{1/\pi}\,\cos(|k|\phi) \quad k>0,\end{aligned} \quad (3)$$

where i, j, and k are all *integers*. The total basis size is then $(2\times n_\phi+1)\times(n_e+1)\times(n_e+2)$, which can be further factored into symmetry blocks of the C_{3v} vibronic group.[1] Note that the use of integral quantum numbers in this basis differs from the case where $E\otimes e$ Jahn–Teller problem is reduced to the angular coordinate of the lower adiabatic potential energy surface. In this case one is solving a vibrational problem on a single surface and half-odd-integral quantum numbers are required to force a sign change in the vibrational wave functions every 2π. In the present case an adiabatic separation of potentials is not possible.

B. The torsional potential

The torsional motion of the –OH group in 9-hydroxytriptycene is related to that of methanol with additional interactions expected between the –OH and nearest H on each benzene moiety. The internal rotation constant B in $\mathbf{H_0}$ of Eq. (1) is equal to $h^2/8\pi^2cI$ where I is the moment of inertia. For coaxial symmetric rotors $I=I_1I_2/(I_1+I_2)$ and from trigonometry one obtains $I=0.624$ amu Å^2 for methanol. For triptycene $I_{\mathrm{TRIP}}\gg I_{\mathrm{OH}}$ giving $I\sim I_{\mathrm{OH}}=0.764$ amu Å^2. This gives the value of $B=22.0\ \mathrm{cm}^{-1}$. This value for the internal rotational constant is held constant throughout this work; i.e., it is assumed that the moment of inertia for this internal rotation does not change in the excited state. This is an approximation as any geometry change involving the –OH group will greatly change the moment of inertia. However, as the –OH group is not directly part of the chromophore which is electronically excited, the structural changes in the –OH group would also be expected to be small. For methanol, the barrier height to the internal rotation is reported[10] to be $V_3=375\ \mathrm{cm}^{-1}$. To reproduce the ground state splitting of 9-hydroxytriptycene a larger barrier height of $V_3\sim 450\ \mathrm{cm}^{-1}$ was required. The reported value for 9-hydroxytriptycene is $V_3=440\pm 20\ \mathrm{cm}^{-1}$ obtained from the temperature dependence of proton spinlattice relaxation times in the solid state.[11] This agreement between the gas phase and solid state values is probably fortuitous.

C. The interaction between Jahn–Teller and torsional potentials

The coupling part of the vibronic Hamiltonian, $\mathbf{H_{JT\phi}}$, is obtained from considering the –OH motion as derived from an e vibrational mode. If the –OH is initially considered as collinear with the C_3 axis, the two components can be considered as the displacement of the H atom in the xy plane: Q_x and Q_y. The lowest order cross term between the coordinates of the Jahn–Teller (X,Y) and this –OH (Q_x,Q_y) e vibrations can be found from the totally symmetric part of the direct product $E\otimes E$: $[XQ_x+YQ_y]$. Rewriting Q_x and Q_y in polar coordinates, $Q_x=R\cos\phi$ and $Q_y=R\sin\phi$, one then restricts this –OH motion to have a fixed value of $R=[Q_x^2+Q_y^2]^{1/2}$. The coordinate R is the C–O–H bend away

from the C_3 axis. A constant R assumes that the C–O–H is bent at a fixed angle. This R value is then subsumed into the coupling constant, B_1, and one obtains the term given in Eq. (1): $H_{JT\phi}=B_1[X\cos\phi+Y\sin\phi]$.

This term then appears on the diagonal of the vibronic Hamiltonian given in Eq. (1). We remove the R coordinate because of the large vibronic basis sets must be used and reducing the vibrational dimension from four to three greatly reduces the computational burden. Also it is clear that the COH bond is bent and the internal rotation, ϕ, of the –OH group turns out to be the most important part of the present problem. The assumption of a constant R reduces the multimode $E\otimes(e\oplus e)$ vibronic problem to a ''$E\otimes(e\oplus\phi)$'' problem. The reduction of the full $E\otimes e$ Jahn–Teller problem to the angular coordinate was first made in a landmark paper by O'Brien.[12] The explicit removal of R from the Hamiltonian also assumes that it is the same in both ground and excited electronic states. The form of the –OH internal rotation mode is given in Fig. 1(b); the harmonic frequency is calculated to be 322 cm^{-1}. from MOPAC/AM1 calculations,[13] though the hindered rotation potential will be very anharmonic. The first $A\rightarrow A$ transition for the fitted ground state internal rotation parameters ($B=22\ cm^{-1}$, $V_3=450\ cm^{-1}$) is calculated to be 280 cm^{-1} (see below).

D. Fitting the parameters

The energies and vibronic wave functions that result from the diagonalization of the vibronic Hamiltonian are used to construct a spectrum to compare with experiment. The full vibronic basis consisted of 47 300 functions ($n_\phi=12$, $n_e=42$). The square of the differences of between calculated and observed energies and intensities, Δ^2, was minimized in parameter space using the principal axes method.[14] Only 27 of the observed spectral bands were used in the fit (see Table I). The energies and intensities were given the weights 1.0 and 0.2, respectively, due to the greater experimental uncertainty in the observed intensities. The 27 levels were fitted with $\Delta^2=48$. Parameters other than those discussed below were initially given the values found for triptycene. **hν**: The value of $h\nu$ is fixed at 63.6 cm^{-1} from the value observed in the harmonic progression seen in the fluorescence spectra (Figs. 3–5). **V_3**: The barrier height of the ground state torsional potential, $V_3(g)$, is determined by the observed ''hot bands'' which occur ~2.6 cm^{-1} to lower energy of each transition in the experimental spectrum. The energy is equal to the difference of the S_0 and S_1 state tunneling splittings. The cold bands are $A\rightarrow E$ transitions and the hot bands a combination of both $E\rightarrow E$ and $E\rightarrow A$ transitions. The splitting between the $E-A$ in the excited state is far smaller than the experimental resolution, so the 2.6 cm^{-1} is essentially the $A-E$ ground state splitting. A value of 450 cm^{-1} was found to give the correct ground state splitting and this was also initially used for the excited state $V_3(e)$. **B_1**: The spectra were simulated for many values for B_1 in the excited state, both positive and negative. The essential behavior is best illustrated by considering the lowest $E-A$ pair of levels from both the $E\otimes e$ and ϕ parts of the problem as shown in Fig. 6. For levels localized below the barrier, the splitting between the E and A states is small. When the $E\otimes e$ and ϕ problem is considered together there are $(E+A)\times(A+E)=2A+B+3E$ levels. With no interaction ($B_1=0$) the energy of these levels are simply the sum of the energies of the separate levels, as shown in Fig. 6(a). When the interaction is turned on, ($B_1\neq 0$) as shown at the left and right hand sides of Fig. 6(b), the levels separate into three groups. For negative B_1 (for the choice of signs of A_1 and A_2 used here) there is an $E-A$ group below two close lying $E-A$ groups at higher energy [Fig. 6(b) left-hand side]. For positive B_1 the situation is reversed, there are two close lying $E-A$ groups and another at higher energy [Fig. 6(b) right-hand side].

This can be rationalized as follows. The vibronic levels in the torsional potential will be strongly localized about the values of $\phi=0°$, 120°, 240°. If one considers the molecule fixed at $\phi=0°$, then both the geometry of the molecule and that of the vibronic Hamiltonian is lowered to C_s. For a *fixed* ϕ, the B_1 parameter would describe the symmetry lowering $C_{3v}\rightarrow C_s$, analogous to the strain term used in the interpretation of the triptycene van der Waals complexes.[3] For a fixed value of ϕ, the equivalence of the three minima in the E⊗e Jahn–Teller problem is removed, making two different from the other. For positive B_1, one minimum is lowered and the other two minima are raised in energy; while for negative B_1, two minima are lowered and one minimum raised.

The energy separation between the close lying pair of the $E-A$ groups of states and the other $E-A$ group is then a measure of the energy difference between the two equivalent minima and the unique minimum of the $E\otimes(e\oplus\phi)$ potential energy surface. The energy separation between the close lying pair of $E-A$ groups, on the other hand, is related to the tunneling splitting between the two equivalent minima.

In the low temperature limit only $A\rightarrow E$ transitions will be observed. Therefore, the triptycene spectrum is expected to ''triple'' upon the addition of the –OH group. For positive B_1, each transition of the triptycene spectrum will be replaced by two closely spaced transitions, with an extra transition to higher energy. For negative B_1, the opposite will occur; for each transition of the triptycene spectrum there will be two additional closely spaced transitions to higher energy. Note that two values of B_1 are needed, $B_1(g)$ for the electronic ground state and $B_1(e)$ for the electronic excited state.

In the present case, after many simulations it was found that $B_1(e)$ is negative in the excited state. The lowest E vibronic level of the $E\otimes e$ S_1 state of triptycene becomes the three S_1 state levels of TOH, accessed in the transitions **a_2**, **e_2**, and **e_3** as indicated in Figs. 6(b) and 7. These three transitions are to the E vibronic levels on the left-hand side of Fig. 6(b). Crucial to the fitting of the spectrum is the coupling constant in the ground electronic state $B_1(g)$. Without this term the intensities of the transitions are completely wrong, as the effect of $B_1(e)$ in the excited state is to shift each minimum to larger values of ρ. This results in very low intensities for the low energy part of the spectrum. However, if $B_1(g)$ is also included, it can be varied so that the intensities can be well reproduced. **V_3(e)**: It was also noticed that

TABLE I. Measured and calculated vibronic band positions and intensities in the R2PI spectrum of 9-hydroxytriptycene relative to the $S_1 \leftarrow S_0$ electronic origin at 36 333.4 cm^{-1}. Experimental levels used in the calculation are marked with an asterisk. The parameters used in the calculation are given in Table II. The quantum numbers given in the assignments are approximate only. All calculated levels are included up to 200 cm^{-1}, after which only those with intensity >0.10 are included in the table. The approximate quantum numbers $(n_\rho, n_\theta, n_\phi)$ are discussed in the text.

	Experimental		Calculated		
Band label	$\Delta\nu$ (cm^{-1})	Relative intensity	$\Delta\nu$ (cm^{-1})	Relative intensity	Assignment $(n_\rho, n_\theta, n_\phi)$
$\mathbf{a_1^*}$	−2.6	0.36	−2.66	0.22	$E \rightarrow E(0,0,0)$
			−2.66	0.22	$E \rightarrow A(0,0,0)$
$\mathbf{a_2^*}$	0.0	1.0	0.0	1.00	$A \rightarrow E(0,0,0)$
$\mathbf{b_1^*}$	32.6	2.1	32.25	1.13	$E \rightarrow E(1,0,0)$
			32.26	1.12	$E \rightarrow A(1,0,0)$
$\mathbf{b_2^*}$	35.4	6.2	34.91	5.30	$A \rightarrow E(1,0,0)$
$\mathbf{c_1}$	⋯	⋯	54.45	0.01	$E \rightarrow B(0,1,0)$
			54.45	0.01	$E \rightarrow E(0,1,0)$
$\mathbf{c_2}$	57.8	0.2	57.11	0.04	$A \rightarrow E(0,1,0)$
$\mathbf{d_1^*}$	67.0	5.2	66.36	2.68	$E \rightarrow E(2,0,0)$
			66.41	2.65	$E \rightarrow A(2,0,0)$
$\mathbf{d_2^*}$	69.5	10.9	69.02	12.90	$A \rightarrow E(2,0,0)$
$\mathbf{e_1^*}$	79.8	1.4	79.77	0.65	$E \rightarrow E(0,0,1^+)$
			79.87	0.71	$E \rightarrow B(0,0,1^+)$
$\mathbf{e_2^*}$	82.3	4.0	82.02	0.17	$E \rightarrow A(0,0,1^-)$
			82.17	0.21	$E \rightarrow E(0,0,1^-)$
			82.43	3.61	$A \rightarrow E(0,0,1^+)$
$\mathbf{e_3^*}$	84.4	1.3	84.83	0.84	$A \rightarrow E(0,0,1^-)$
	⋯	⋯	88.37	0.002	$E \rightarrow E(1,1,0)$
			88.38	0.003	$E \rightarrow B(1,1,0)$
			91.03	0.012	$A \rightarrow E(1,1,0)$
$\mathbf{f_1^*}$	100.0	4.4	100.5	2.57	$E \rightarrow E(3,0,0)$
			100.5	2.57	$E \rightarrow A(3,0,0)$
$\mathbf{f_2^*}$	102.6	9.4	103.1	12.75	$A \rightarrow E(3,0,0)$
$\mathbf{g_1^*}$	108.8	1.8	111.2	1.29	$E \rightarrow E(1,0,1^+)$
			111.3	1.34	$E \rightarrow B(1,0,1^+)$
$\mathbf{g_2^*}$	111.4	3.8	111.5	0.03	$E \rightarrow E(0,2,0)$
			111.5	0.03	$E \rightarrow A(0,2,0)$
			113.9	6.52	$A \rightarrow E(1,0,1^+)$
$\mathbf{g_3^*}$	113.8	1.6	114.1	0.13	$A \rightarrow E(0,2,0)$
	120.2	0.3	120.3	0.07	$E \rightarrow A(1,0,1^-)$
			120.5	0.09	$E \rightarrow E(1,0,1^-)$
*	123.7	0.6	122.0	0.16	$E \rightarrow B(2,1,0)$
			122.0	0.16	$E \rightarrow E(2,1,0)$
			123.1	0.44	$A \rightarrow E(1,0,1^-)$
*	126.7	1.3	124.7	0.85	$A \rightarrow E(2,1,0)$
	133.7	0.4	135.7	0.00	$E \rightarrow B$
			135.8	0.00	$E \rightarrow E$
			136.6	0.06	$E \rightarrow E$
			136.6	0.07	$E \rightarrow A$
	136.4	1.3	138.4	0.00	$A \rightarrow E$
			139.2	0.30	$A \rightarrow E$
$\mathbf{h_1^*}$	138.9	5.2	139.8	1.49	$E \rightarrow E(4,0,0)$
			139.9	1.52	$E \rightarrow A(4,0,0)$
$\mathbf{h_2^*}$	141.9	8.4	142.4	7.62	$A \rightarrow E(4,0,0)$
	⋯	⋯	146.0	0.01	$E \rightarrow E(1,2,0)$
			146.0	0.01	$E \rightarrow A(1,2,0)$
			148.7	0.05	$A \rightarrow E(1,2,0)$
$\mathbf{i_1^*}$	147.5	2.6	150.0	1.20	$E \rightarrow E(2,0,1)$
			150.1	1.21	$E \rightarrow B(2,0,1)$
$\mathbf{i_2^*}$	150.4	4.3	152.7	5.89	$A \rightarrow E(2,0,1)$
	160.8	1.6	158.4	0.21	$E \rightarrow B$
			158.5	0.22	$E \rightarrow E$
			163.4	0.04	$E \rightarrow A$
			163.6	0.06	$E \rightarrow E$
	163.6	3.4	161.1	1.13	$A \rightarrow E$
			166.2	0.29	$A \rightarrow E$
			168.3	0.01	$E \rightarrow B(0,3,0)$
	⋯	⋯	168.3	0.00	$E \rightarrow E(0,3,0)$
			171.0	0.02	$A \rightarrow E(0,3,0)$
	167.3	1.4	170.4	0.28	$E \rightarrow E$
			170.5	0.29	$E \rightarrow A$
*	170.0	3.1	173.0	1.52	$A \rightarrow E$
*	174.2	0.3	174.4	0.22	$E \rightarrow E$
			174.4	0.22	$E \rightarrow B$
*	177.2	0.7	177.0	1.00	$A \rightarrow E$
*	180.2	1.6	180.7	0.44	$E \rightarrow E$
			180.8	0.48	$E \rightarrow A$
*	183.0	4.1	183.4	2.40	$A \rightarrow E$
	184.7	0.5	185.9	0.42	$E \rightarrow E$
			185.9	0.40	$E \rightarrow B$
*	188.6	0.5	187.8	0.13	$E \rightarrow E$
			187.9	0.15	$E \rightarrow A$
			188.5	1.93	$A \rightarrow E$
	190.6	1.6	190.5	0.82	$A \rightarrow E$
			193.6	0.92	$E \rightarrow E$
			193.7	0.90	$E \rightarrow B$
*	193.4	3.6	196.2	4.38	$A \rightarrow E$
			197.7	0.00	$E \rightarrow A$
	⋯	⋯	197.8	0.00	$E \rightarrow E$
			200.5	0.00	$A \rightarrow E$
	197.3	0.5	199.0	0.28	$E \rightarrow B$
			199.0	0.30	$E \rightarrow E$
	202.3	1.4	201.7	1.46	$A \rightarrow E$
	205.3	2.8	206.7	0.02	$A \rightarrow E$
	208.7	1.1	209.0	0.08	$E \rightarrow A$
			209.1	0.09	$E \rightarrow E$
	211.2	2.3	211.8	0.52	$A \rightarrow E$
			212.3	0.09	$E \rightarrow E$
			212.4	0.11	$E \rightarrow A$
	⋯	⋯	215.0	0.52	$A \rightarrow E$
			216.5	0.50	$E \rightarrow E$
			216.5	0.50	$E \rightarrow B$
	221.4	0.8	219.1	2.34	$A \rightarrow E$
	224.6	1.5	226.7	0.19	$E \rightarrow E$
			226.7	0.23	$E \rightarrow A$
	227.3	1.4	227.5	0.22	$A \rightarrow E$
			229.4	1.24	$A \rightarrow E$
	231.0	2.0	229.7	0.47	$E \rightarrow B$
			229.7	0.51	$E \rightarrow E$
			230.7	0.10	$E \rightarrow E$
			230.7	0.12	$E \rightarrow A$
	233.7	4.8	232.4	2.39	$A \rightarrow E$
			233.3	0.60	$A \rightarrow E$
			236.8	1.33	$E \rightarrow E$
			236.9	1.30	$E \rightarrow B$
	237.4	1.1	239.4	6.19	$A \rightarrow E$
	247.9	0.7	248.1	0.12	$E \rightarrow B$
			248.2	0.14	$E \rightarrow E$
	250.3	0.9	250.8	0.69	$A \rightarrow E$
			251.2	0.14	$A \rightarrow E$
			251.5	0.11	$E \rightarrow E$
			251.5	0.11	$E \rightarrow B$
	255.4	0.4	254.2	0.53	$A \rightarrow E$
	257.9	0.9	258.0	0.36	$A \rightarrow E$
	261.6	0.7	259.1	0.68	$E \rightarrow E$
			259.1	0.74	$E \rightarrow B$
			261.6	0.65	$A \rightarrow E$
	264.7	2.5	261.7	2.87	$A \rightarrow E$
	268.1	2.0	266.2	0.15	$A \rightarrow E$
			268.1	0.13	$E \rightarrow E$
			268.1	0.18	$E \rightarrow A$
	271.5	1.2	269.5	0.63	$E \rightarrow E$
			269.5	0.55	$E \rightarrow B$

TABLE I. (*Continued*.)

Band label	Experimental $\Delta\nu$ (cm^{-1})	Experimental Relative intensity	Calculated $\Delta\nu$ (cm^{-1})	Calculated Relative intensity	Assignment $(n_\rho, n_\theta, n_\phi)$
			270.7	1.05	$A \rightarrow E$
	273.9	1.8	272.2	2.62	$A \rightarrow E$
			275.0	0.12	$E \rightarrow E$
			275.1	0.13	$E \rightarrow B$
	⋯	⋯	277.6	0.18	$E \rightarrow B$
			277.6	0.19	$E \rightarrow E$
			277.7	0.55	$A \rightarrow E$
	281.9	0.3	280.2	0.81	$A \rightarrow E$
	284.9	0.9			
	293.0	0.7	301.2	0.39	$E \rightarrow B$
			301.2	0.39	$E \rightarrow E$
	295.6	1.4	303.9	1.74	$A \rightarrow E$
			309.0	0.15	$A \rightarrow E$
	⋯		318.9	0.23	$A \rightarrow E$
	⋯		327.5	0.19	$A \rightarrow E$
	⋯		337.9	0.25	$A \rightarrow E$
	⋯		341.6	0.34	$A \rightarrow E$

the splitting between $\mathbf{e_2}$ and $\mathbf{e_3}$ calculated initially was too large and the intensity of the $\mathbf{e_3}$ transition too low. However both these points improved when the torsional barrier height in the excited state, $V_3(e)$, was increased. It was found that the barrier height was required to be much larger than in the ground electronic state, but the fitted value of $V_3(e)$ ~1000 cm^{-1} must be regarded as approximate. $\mathbf{K_2}$, $\mathbf{A_1}$, $\mathbf{A_2}$: The parameters discussed above are also dependent on the normal $E \otimes e$ Jahn–Teller parameters K_2, A_1, A_2 which are also allowed to vary. There is then a seven dimensional parameter space to search in a least squares fit of the experimental data. This become computationally intensive without some of the strategies outlined above.

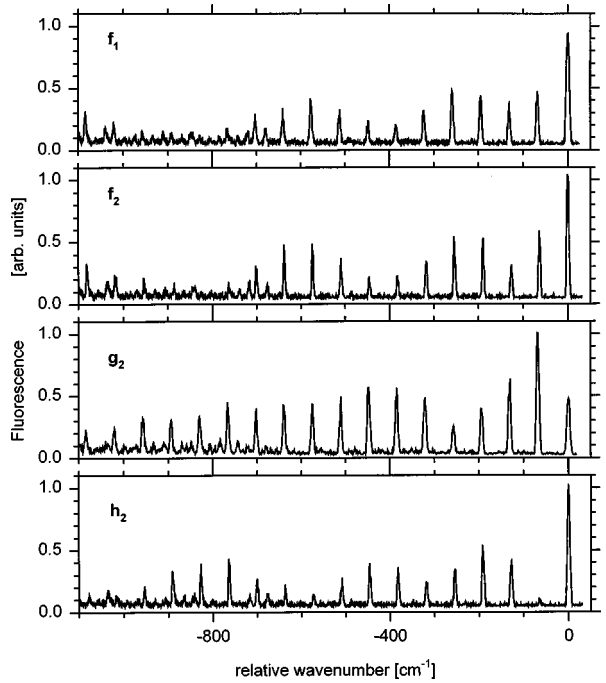

FIG. 5. The single vibronic level fluorescence emission spectra of TOH excited to levels $\mathbf{f_1}$, $\mathbf{f_2}$, $\mathbf{g_2}$, and $\mathbf{h_2}$. The abscissa is relative to the excitation energy.

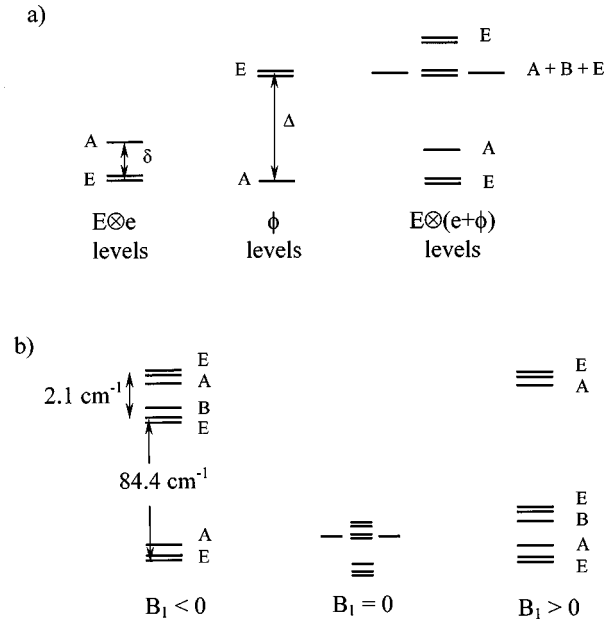

FIG. 6. A schematic diagram of the vibronic energy levels of the excited electronic E state. (a) $B_1 = 0$, no interaction. The energy differences δ and Δ are tunnelling splittings due to the Jahn–Teller motion and internal rotation respectively when these are considered separately. (b) $B_1 \neq 0$. The indicated splittings for $B_1 < 0$ are obtained using the final fitted parameters (see Table II). Note that only transitions into the E vibronic levels are symmetry allowed in the low temperature limit.

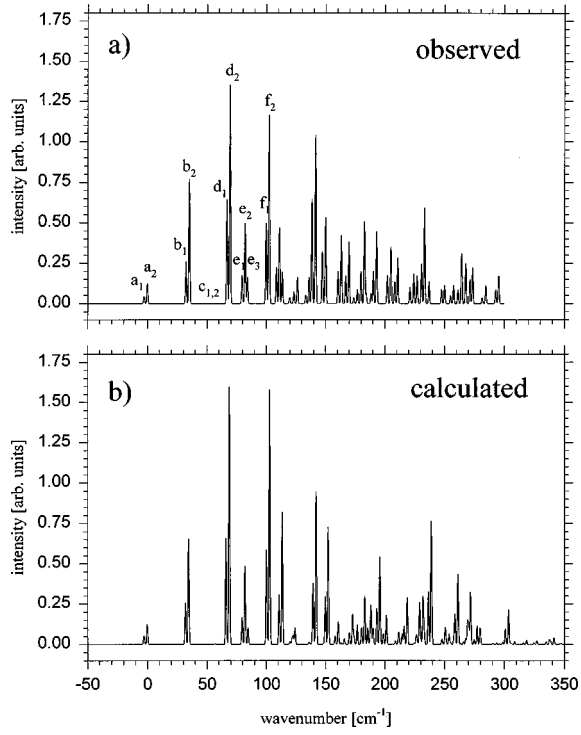

FIG. 7. The calculated absorption spectrum compared with the measured R2PI spectrum. The experimental spectrum has been constructed using the energies and intensities given in Table I. The stick spectra have been convoluted with a 1 cm^{-1} half-width Gaussian to aid the comparison.

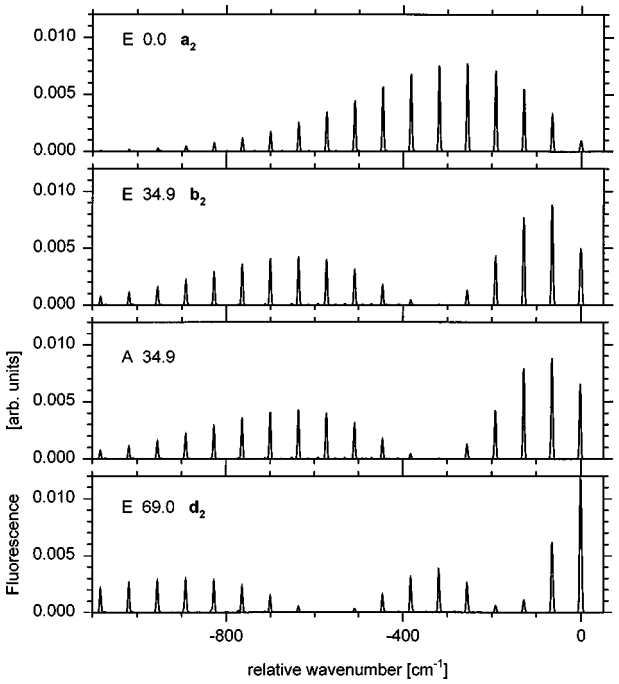

FIG. 8. The calculated single vibronic level fluorescence emission spectra of TOH from levels $\mathbf{a_2}$, $\mathbf{b_1}$, $\mathbf{b_2}$, and $\mathbf{d_2}$, using the parameter set given in Table II. The calculated intensity pattern is to be compared with the observed spectra shown in Fig. 3.

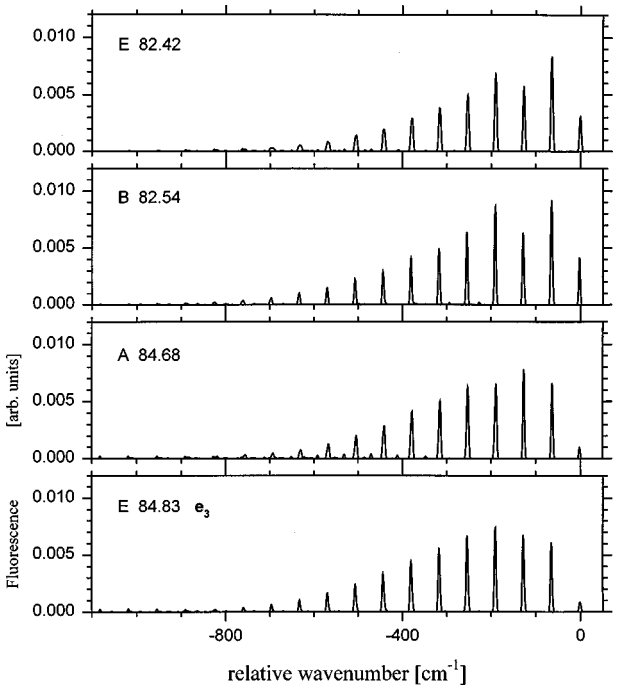

FIG. 9. The calculated single vibronic level fluorescence emission spectra of TOH from levels $\mathbf{e_1}$, $\mathbf{e_2}$, and $\mathbf{e_3}$. The calculated intensity pattern is to be compared with the observed spectra shown in Fig. 4.

IV. DISCUSSION

A. Comparison of calculated and observed R2PI spectra

The measured R2PI spectrum is compared with the calculated absorption spectrum in Fig. 7. A complete listing of the positions and intensities of the experimental bands are given Table I. The intensities of the bands are relative to the origin at $\mathbf{a_2}$. Both the calculated and the ''observed'' spectra in Fig. 7 are constructed from convolution of the ''stick'' spectra with a 1.0 cm^{-1} full width at half height Gaussian. This is because many of the experimental peaks are assigned to multiple unresolved calculated peaks. The position and intensity of all the calculated bands up to 200 cm^{-1} above the origin are also given in Table I. Above 200 cm^{-1}, only transitions calculated to have a relative intensity >0.1 are given.

The transitions are assigned according to the C_{3v} vibronic group. At low temperature only $A \rightarrow E$ transitions are allowed. When the internal rotation level E is populated in the S_0 state, transitions to all excited levels, $E \rightarrow A$, B and E are formally allowed. Also included in Table I are approximate quantum numbers that can be given to the lowest vibronic levels. These assignments can be made from examining the nodal structure of the vibronic probability functions. Practically all features of the experimental spectrum can be reproduced in the calculation. However, there are some discrepancies between the observed and calculated intensities to higher energy.

B. Comparison of calculated and observed emission spectra

The calculated emission spectra shown in Figs. 8–10 can be compared to the observed spectra in Figs. 3–5. Again, the calculated spectra have been convoluted with a 1 cm^{-1} FWHH Gaussian to aid the comparison, as each of the ''bands'' can be composed of many individual transitions. As with the fluorescence of triptycene, the nodal structure in the emission spectra reflects the nodal structure in the radial

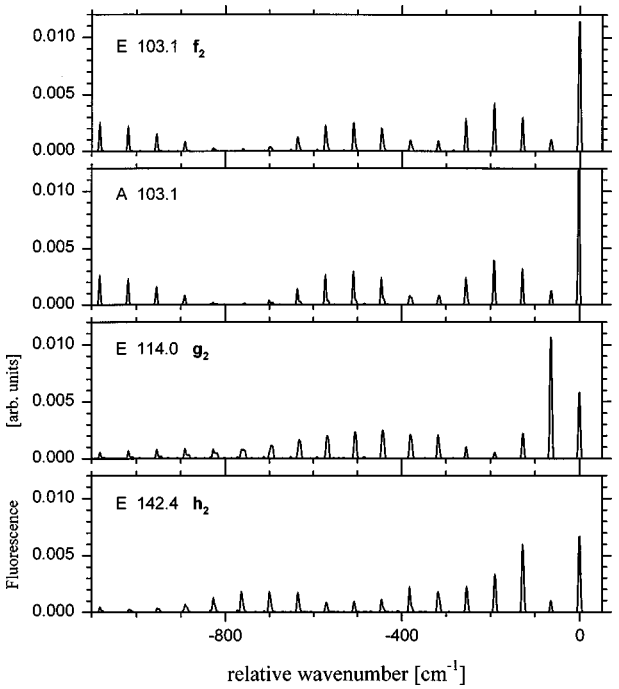

FIG. 10. The calculated single vibronic level fluorescence emission spectra of TOH from levels $\mathbf{f_1}$, $\mathbf{f_2}$, $\mathbf{g_2}$, and $\mathbf{h_2}$. The calculated intensity pattern is to be compared with the observed spectra shown in Fig. 5.

TABLE II. Parameters of the $E\otimes e$ Jahn–Teller vibronic Hamiltonian. An asterisk denotes a parameter that has been allowed to vary. The last column contains the values found for triptycene (Ref. 1).

Parameter [cm^{-1}]	9-hydroxytriptycene	triptycene
ground state		
$h\nu(g)$	63.6	64.2
$B(g)$	22.0	···
$V_3(g)^*$	450.0	···
$B_1(g)^*$	−45.0	···
excited state		
$h\nu(e)$	47.855	47.83
K_2^*	47.855	47.83
A_1^*	−70.295	−78.92
A_2^*	−10.803	−10.164
$B(e)$	22.0	···
$V_3(e)^*$	1000.0	···
$B_1(e)^*$	−20.952	···

(ρ) direction of the excited state vibronic wave functions. The experimental emission spectra observed following excitation at bands $\mathbf{a_2}$, $\mathbf{b_2}$, and $\mathbf{d_2}$ in Fig. 3 can be compared directly with the calculated emission in Fig. 8. This is because exciting into the higher of each pair of transitions, i.e., the cold band, only excites a single E vibronic state. Exciting into the lower hot band $\mathbf{b_1}$, on the other hand, actually accesses the excited state levels of E and A symmetry both at $\sim$34.9 cm^{-1}. The calculated emission from both these levels is very similar. The ''$\mathbf{b_1}$'' emission is also observed to be very similar to the ''$\mathbf{b_2}$'' emission, which accesses the E excited state only. The nodal pattern of bands **a**, **b**, and **d** correspond to the $n_\rho=0$, 1, 2 approximate quantum numbers given in Table I. The maximum in the observed emission when exciting into band $\mathbf{a_2}$ is at $n=2$ ground state quanta. This is different from the $n=4$ maximum calculated, and we attribute this to experimental difficulties in exciting the weak $\mathbf{a_2}$ band.

The emission from exciting into the **e** levels is interesting in that Franck–Condon patterns are reproduced in detail. The direct comparison is complicated as exciting into bands $\mathbf{e_1}$, $\mathbf{e_2}$, and $\mathbf{e_3}$ actually excite the levels [$E(82.42)$, $B(82.54)$], [$A(84.68)$, $E(84.83)$, $E(82.43)$], and [$E(84.83)$], respectively, by unequal amounts (see Table I). Also, it is not known what population redistribution may occur between the levels after excitation. However, as before, emission from a vibronic singlet (A or B) is very similar to that of the nearby E state. Both the short Franck–Condon pattern and the alternating intensities seen when exciting into the **e** bands are reproduced.

The observed and calculated emission obtained from exciting into other levels are shown in Figs. 5 and 10, respectively. Again, the nodal structure in band **f** is reproduced (3 minima in the emission). Other features such as strong/weak first member of the progression of bands $\mathbf{g_2}/\mathbf{h_2}$, respectively, are correctly reproduced in the calculation. The parameters of the vibronic model have not been varied to fit the observed emission spectra. The calculated spectra are obtained using the parameters given in Table II obtained from fitting the R2PI spectrum.

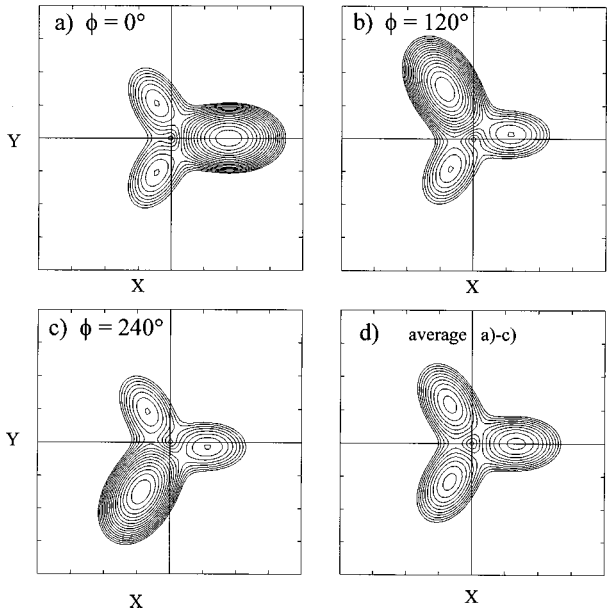

FIG. 11. The lower the adiabatic potential energy surface of the S_1 state plotted as a function of the dimensionless Jahn–Teller coordinates X and Y for fixed values of (a) ϕ=0°, (b) ϕ=120°, and (c) ϕ=240° using the parameters given in Table II. (d) The average of the potentials in (a)–(c). The X, Y range is ±8 and the contours are drawn from −150 to 0 cm^{-1} at 10 cm^{-1} equally spaced intervals.

It is interesting to see features additional to the progression in the e vibrational mode appearing in both the observed and calculated emission from these higher levels. In the case of the calculated spectra, this is due to nonzero intensity of the transitions to the first excited torsional vibration. However, it is noted that these additional experimental features beginning at ~ -670 cm^{-1} are much stronger than calculated and may be due to the participation of some other ground state vibration.

C. The potential energy surfaces

Table II lists the parameters of the vibronic Hamiltonian obtained from fitting the R2PI spectrum of 9-hydroxytriptycene as well as those obtain for the $E\otimes e$ problem of bare triptycene. The parameters common to the $E\otimes e$ problem are seen to be quite similar. Figure 11 shows the lower adiabatic potential energy surface of the Jahn–Teller S_1 state as a function of the dimensionless (X,Y) coordinates over the range ±8. Figures 11(a)–11(c) were obtained from diagonalizing the potential energy terms of Eq. (1) with the parameters of Table II at fixed values of ϕ. For a fixed ϕ, the potential energy surface reflects the C_s symmetry of the molecule, while the average of the potentials shown in Fig. 11(d) is very close to that of bare triptycene (Table III). Each surface for fixed ϕ is very similar to that found for the triptycene·Ne van der Waals complex[3] where one minima was made lower than the other two by a Ne atom complexing between two benzene rings. However, in the present case the low symmetry perturbation is dynamic, being due to the internal rotation of the –OH group.

Figure 12 show the lower potential energy surface as a function of the Jahn–Teller pseudorotation, θ, and the hin-

TABLE III. Some energetic and geometrical quantities derived from the parameters of Table II. The last column contains the values found for triptycene (Ref. 1).

Property	TOH (ϕ_0)[a]	TOH ($\langle\phi\rangle$)[b]	triptycene[c]	
$E_{JT}[cm^{-1}]$	158.6 70.6	94.1	113.4	JT stabilization energy
$E_{loc}[cm^{-1}]$	113.6 53.1	58.55	67.77	barrier height
ρ_0	3.48 2.29	2.68	2.87	radial position of minima
ρ_s	1.18 0.71	1.01	1.16	radial position of saddle points
3Γ $[cm^{-1}]$	0.000 69		0.93	tunneling splitting

[a]ϕ_0 denotes for ϕ at a minimum $\phi_0=0°$, 120°, and 240° as in Figs. 11(a)–11(c).
[b]$\langle\phi\rangle$ denotes the values for the potential energy surface taken as the average of the surfaces at $\phi_0=0°$, 120°, and 240° as in Fig. 11(d).
[c]These values have been taken from Ref. 1.

dered OH rotation, ϕ. At each point, the surface is minimized with respect to the radial coordinate ρ since the energy pathway between the minima is far from circular (see Fig. 11). Figure 12(a) uses the parameters of Table II, while that of Fig. 12(b) is for $B_1(e)=0$. For the zero interaction case, there are nine equivalent minima at the 0°, 120°, and 240° positions. After switching on the interaction ($B_1\neq 0$), three minima are lowered with respect to the other six. These minima are slightly shifted from the high symmetry positions, although this is hard to see on the scale of the plots.

The potential energy surface shown in Fig. 12 are cyclic, repeating every 2π. If the sides of the plots at $\phi=\pm\pi$ are joined to form a tube, and the circular ends of this tube are also joined, one forms a contour plot drawn on the surface of a torus. It is instructive to view the potentials in this way as tracing a path around the θ coordinate can be thought to enclose the conical intersection of the Jahn–Teller E state placed at the center of the torus. The path around the ϕ coordinate does not enclose this conical interaction.

The barrier between the minima is very high (~1000 cm^{-1}) along the ϕ coordinate compared to the barriers along the θ coordinate (53.1 and 113 cm^{-1}, respectively, between the equivalent and nonequivalent minima). A simplistic interpretation would be that the large barrier height and small tunneling splitting along the ϕ coordinate would make this –OH rotation appear stationary at the C_s geometry from the point of view of the Jahn–Teller pseudorotation. However, there are not separate tunneling splitting and tunneling rates along the ϕ and θ coordinates. It will be shown that the tunneling motion between the barriers is highly correlated. That is, the Jahn–Teller pseudorotation and the –OH internal rotation move in concert.

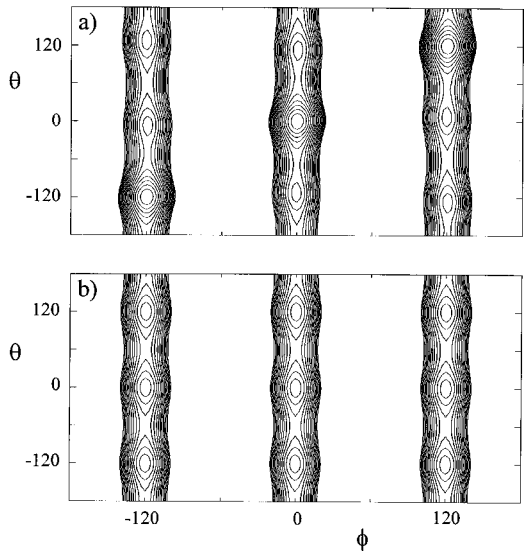

FIG. 12. The lower adiabatic potential energy surface plotted as a function of the Jahn–Teller pseudorotation coordinate θ and the OH torsional coordinate ϕ. The coordinate θ is given by $\theta=\tan^{-1}(Y/X)$. At each point the potential is minimized along the $\rho=\sqrt{X^2+Y^2}$. The contours are equally spaced in 20 cm^{-1} intervals. (a) Using the parameters given in Table II. (b) Using the parameters given in Table II, except setting $B_1=0$.

D. The vibronic wavefunctions.

The calculated vibronic probability functions in (X,Y) space for the first 12 vibronic levels of E symmetry are shown in Figs. 13 and 14. These plots are the sum of the squares of each component of the E vibronic wave function. The probability of the vibronic wave functions along the ϕ coordinate has been integrated out, rather than a fixed value of ϕ being used. The probability functions therefore display the C_{3v} symmetry of the potential shown in Fig. 11(d) rather than that of a fixed value of ϕ. These vibronic probability functions are labeled $\mathbf{a_2}$, $\mathbf{b_2}$,…, corresponding to the probability functions of the upper levels of the observed transitions labeled $\mathbf{a_2}$, $\mathbf{b_2}$,… in Fig. 7, together with their calculated energy relative to the lowest vibronic level. The nodal structure of the vibronic functions show the approximate radial and angular quantum numbers n_ρ and n_θ given in Table I. The radial nodes are clearly reflected in the intensity pattern of the emission spectra shown in Figs. 3–5. For example, the emission from levels $\mathbf{a_2}$, $\mathbf{e_2}$, and $\mathbf{e_3}$ all have no nodes in their intensity patterns, while emission from levels $\mathbf{b_2}$ and $\mathbf{d_2}$ have one and two nodes, respectively, in agreement with the probability functions.

Figure 15 shows some of the calculated vibronic probability functions of E symmetry at higher energies which

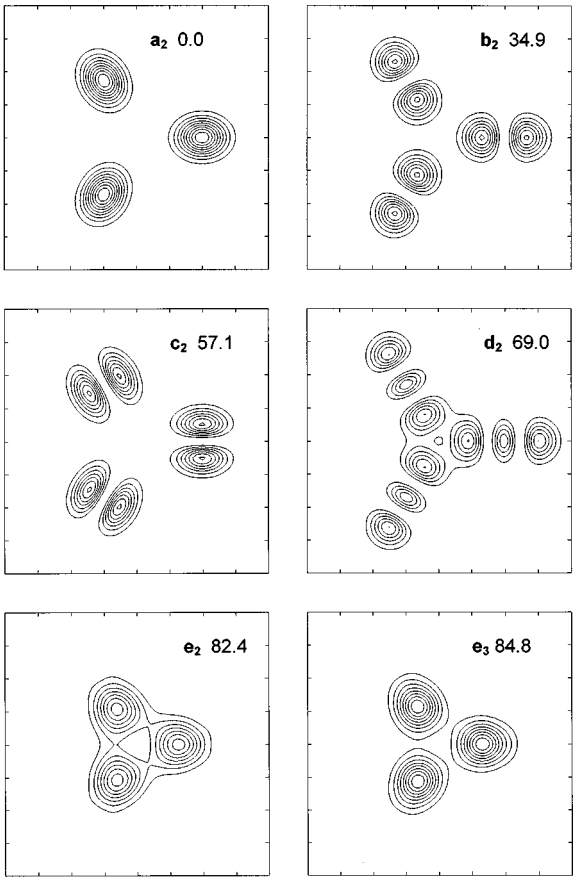

FIG. 13. The calculated vibronic probability functions in (X,Y) space for the first six vibronic levels of E symmetry calculated using the parameter set given in Table II. For each point the vibronic probability function has been integrated along ϕ. The nodal structure of the vibronic probability functions shows the approximate radial and angular quantum numbers n_ρ, n_θ given in Table I. The radial nodes is clearly reflected in the intensity pattern of the emission spectra shown in Figs. 3–5. The contour intervals are equally spaced by 0.015.

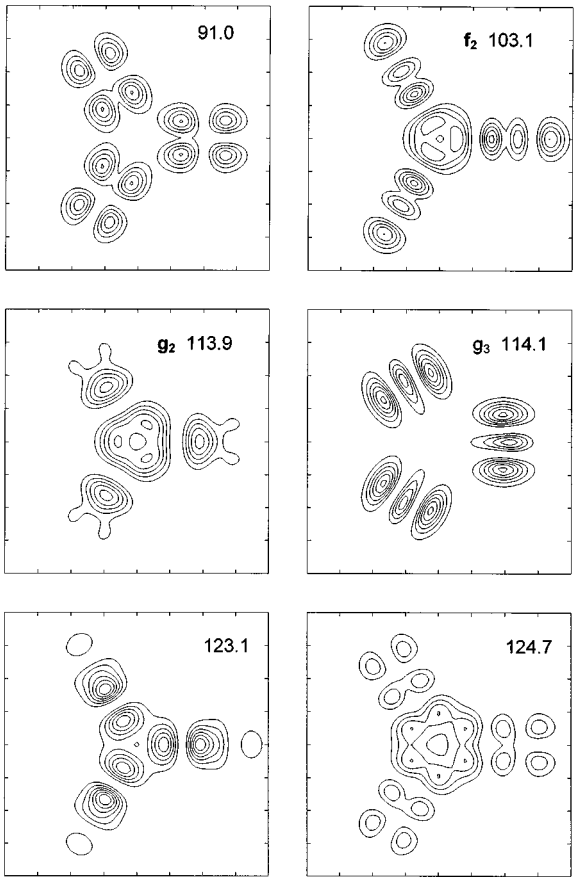

FIG. 14. The calculated vibronic probability functions for the 7–12 vibronic levels of E symmetry. See also caption to Fig. 13.

have a large intensity in the R2PI spectrum. All these functions show a large probability amplitude at small values of $\langle\rho\rangle$. The wave function of such levels will have a high overlap with the ground state wave functions. They can be classify as ''cone states,'' belonging predominately to the upper sheet of the Jahn–Teller potential energy surface, although in each case there also appears substantial probability *between* the lower and upper sheets of the $E\otimes(e\oplus\phi)$ surface.

The vibronic probability functions $\mathbf{a_2}$, $\mathbf{c_2}$, and $\mathbf{g_3}$ correspond to $n_\theta=0$, 1, and 2 and show little mixing with either the n_ρ or n_ϕ type modes. The E vibronic probability function at 171.0 cm^{-1} (not shown) corresponds to a clear $n_\theta=3$ case. The probability functions $\mathbf{e_2}$ and $\mathbf{e_3}$ are similar to that of the lowest vibronic function $\mathbf{a_2}$, except that the average value of ρ is smaller. This is because these vibronic wave functions are localized in the upper two minima of the potentials as viewed with a fixed value of ϕ [Figs. 11(a)–11(c)]. In other words, the $\mathbf{a_2}$ wave function is localized in the minimum that the–OH mode makes lowest ($\theta=0°$, for $\phi=0°$), while the $\mathbf{e_2}$ and $\mathbf{e_3}$ wave functions localize in the upper minima ($\theta=120°$ and 240°, for $\phi=0°$).

The extent of correlation of the wavefunctions in (θ,ϕ) space is shown in Fig. 16. Here the probability functions have been integrated along the ρ coordinate, so they are not distorted by being evaluated at a fixed value of ρ. For levels below the barrier heights, the θ and ϕ motions are highly correlated; while at higher energy the levels are more evenly distributed over (θ,ϕ) space. The trend is clearly seen in the probability plots of $\mathbf{a_2}$, $\mathbf{d_2}$ and $\mathbf{f_2}$, $\mathbf{g_2}$ of Fig. 16. This correlation implies that *the motion of the Jahn–Teller pseudorotation is enslaved to the–OH internal rotation*; the butterfly flapping of the benzene rings follows the minimum generated by the position of the–OH group. Tunneling will occur along the diagonal of the probability plots, not along the θ coordinate as might be implied by the lower barrier height in this direction. For the higher energy levels, the more even distribution over (θ,ϕ) space implies that the position of the–OH group is less important in determining which benzene ring will be brought closer together.

The behavior of the vibronic probability functions $\mathbf{e_2}$ and $\mathbf{e_3}$ are similarly understood as being localized in the higher energy minima generated for a fixed value of ϕ. For bare triptycene, each of the three equivalent Jahn–Teller minima corresponds to a large angle change between two of the three benzene rings [Q_x of Fig. 19(a)]. In TOH one minimum is lowered with respect to the other two minima for a *fixed* value of ϕ [see Fig. 11(a)]. Each of these two higher energy minima are the Jahn–Teller minima with the large angle change between two benzene rings which do not include the–OH group. The lower minima of Fig. 11(a) corresponds

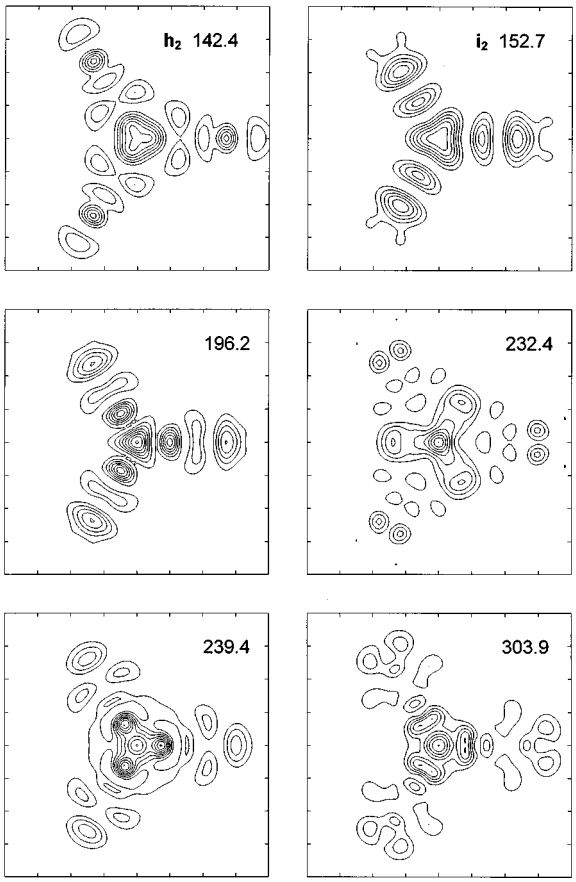

FIG. 15. Some higher calculated vibronic probability functions of E symmetry which show large intensity in the R2PI spectrum. Note the large probability amplitude at small values of $\langle\rho\rangle$ which classify these as cone states, belonging predominately to the upper sheet of the Jahn–Teller potential energy surface.

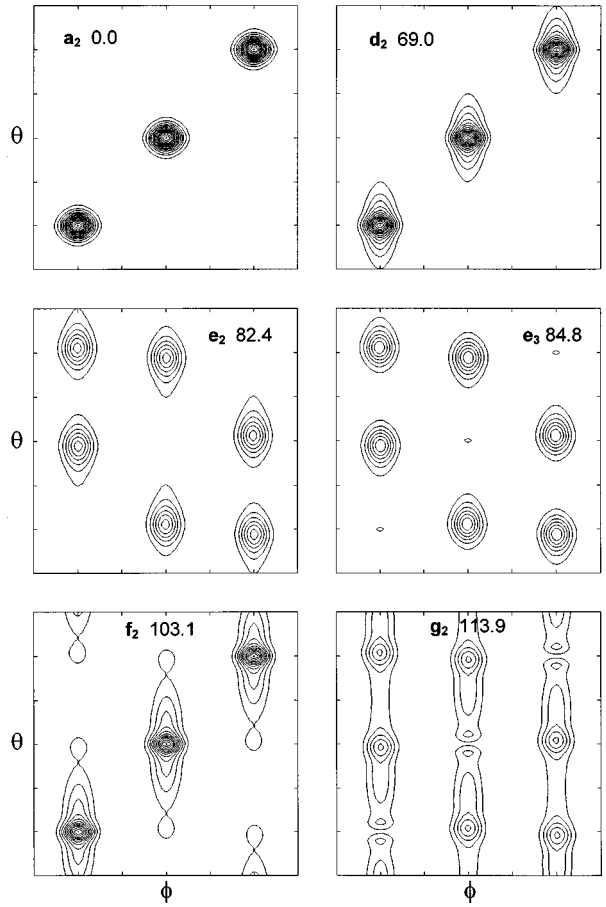

FIG. 16. Some calculated vibronic probability functions of E symmetry as a function of the Jahn–Teller pseudorotation (θ) and the internal rotation-OH (ϕ). The range is $\pm\pi$ along each axis. The contour intervals are equally spaced by 0.1.

to the Jahn–Teller minima with the large angle change between the two benzene rings which bracket the–OH group. It is also clear that the $\mathbf{e_2}$ and $\mathbf{e_3}$ wave functions represent symmetric and antisymmetric combinations of the wavefunctions localized in each well. This can be seen in Fig. 16 where the probability contours about each minima of the vibronic function $\mathbf{e_2}$ join, whereas those of $\mathbf{e_3}$ fall to zero between the minima. Similar symmetric/antisymmetric behavior is displayed in the probability plots as a function of ϕ (not shown), although in this case the large barrier heights make this harder to see. This symmetric/antisymmetric behavior is indicated with $\pm$ superscripts respectively on the n_ϕ approximate quantum number for levels with their wave functions localized in the upper minima.

The probability plots shown in Fig. 16 can also be viewed as being on the surface of the torus introduced in the previous section for the potential energy surface. A path around the θ coordinate encloses the conical intersection at the center of the torus, while a circuit around the ϕ coordinate does not. It is well known that the electronic and vibrational parts of a vibronic wave function both change sign after a circuit in coordinate space returns to the same geometry and encloses a conical intersection.[15] This is a molecular manifestation of Berry's geometric phase[16] and is required for the total vibronic wave function to remain single valued. In the $E\otimes(e\oplus\phi)$ model used here, a circuit of 2π about θ will cause a wave function to acquire a Berry's phase, while a circuit about ϕ will not. However in the present case the θ and ϕ motions are concerted according to Fig. 16. In the lowest vibronic wave function of the S_1 state of TOH the tunneling motion will simultaneous change both θ *and* ϕ from 0 to 2π describing a closed spiral on the surface on the torus. This vibronic wave function would then be expected to acquire a Berry's phase from this tunneling motion. Recently there has been speculation on whether the triptycene molecule would present a good candidate for optical tests for Berry's phase.[17] The present molecule would be an even better candidate, enslaving the Jahn–Teller pseudorotation to the motion of an internal rotation has slowed it down by many orders of magnitude. The calculated tunneling splitting is reduced from 0.93 to 0.000 69 cm^{-1} on going from triptycene to 9-hydroxytriptycene.

E. Extensions to the $E\otimes(e\oplus\phi)$ model

The model potential energy surface that has been used in Eq. (1) is extremely simplistic and it is surprising that it captures so much of the spectroscopic behavior. We have used a harmonic vibrational potential for both ground and excited electronic states, with first- and second-order Jahn–Teller coupling in the excited E state. The torsional potential

is characterized by a single term and only the lowest order coupling between e and ϕ vibrational modes has been included. A close examination of the differences between the calculated and measured spectra suggests how an improved effective molecular Hamiltonian may differ from this model.

A general feature of the spectrum is that bands at a greater shift from the origin were always calculated to be too high in frequency. Since these higher energy features access regions of the potential energy surface with greater values of ρ, the potential surfaces should ''soften'' at higher values of ρ. This behavior was also observed for the $E\otimes e$ model of bare triptycene. For triptycene, a much better fit was achieved by extending the $E\otimes e$ model to a $(A\oplus E)\otimes e$ model. The interaction with the higher lying excited A electronic state softened the higher energy parts of the potential energy surface. However, it is not clear whether the A electronic state is important in its own right or merely provides a way for the potential energy surface to vary and become closer to its true form. Due to the extremely large basis sizes required, the $(A\oplus E)\otimes e$ model was not used to model 9-hydroxytriptycene.

One part of the R2PI spectrum which was not reproduced well, was the intensity of the $\mathbf{g_3}$ band (Table I, Fig. 7). An examination of the probability function $\mathbf{g_2}$ reveals that it has the approximate quantum numbers $(n_\rho=1, n_\phi=1)$ while $\mathbf{g_3}$ has $(n_\theta=2)$. From Fig. 14, there appears to be very little mixing between the vibration in the θ direction and the other modes. We attempted to rectify this by including higher order coupling terms of A_1 symmetry into the vibronic Hamiltonian: $X\cos 2\phi\ \mathbf{I}$ and $(X^2-Y^2)\cos\phi\ \mathbf{I}$. Neither of these terms made a substantial improvement to the fit.

We also tried terms of the type $\cos 6\phi\ \mathbf{I}$ to alter the torsional potential and an anharmonic term for the e vibration of the form $X(X^2-3Y^2)\ \mathbf{I}$. This later term is of interest as it changes the sign of the distortion of the upper adiabatic potential. This could be important, as the R2PI spectrum probes the ''cone'' states. Both this anharmonic term and the second order Jahn–Teller coupling A_2, in Eq. (1) cause three minima on the lower adiabatic potential energy surface. The A_2 term also causes a bulgè on the opposite sides of the upper surface, while the anharmonic terms will cause the upper surface to bulge on the same side. By comparing the simulated spectra with experiment, it does appear that it is the second order coupling rather than anharmonicity which is important in causing the Jahn–Teller minima in this molecule.

The above extensions to the simple vibronic Hamiltonian given by Eq. (1), only gave marginal improvements to the fit. It was decided to optimize the fit for the simplest model rather than introducing a large number of additional parameters.

F. The geometry of triptycene and 9-hydroxytriptycene in the S_1 state

The geometry of the triptycene molecule at the minima of the $E\otimes e$ potential energy surface is a distortion along the e_x component of the e vibration. In previous work, it has been assumed that the minima correspond to a geometry where the angle between two benzene rings decreases from 120°. Using a calculated reduced mass, the angle change could be quantified as a reduction to 103.5°.[3] Based on consideration of steric repulsion between the–OH hydrogen atom and the proximal benzene hydrogen atoms, the three equivalent minima of the *uncoupled*–OH internal rotation would be expected to correspond to geometries where the–OH group points midway *between* two neighboring benzene rings. If the Jahn–Teller minima in the S_1 state [Fig. 12(a)] would correspond to a reduction of flap angle between two neighboring benzene rings to 103.6°, concurrent with an opening of the two other benzene ring flap angles to 128.2°, then the steric repulsion should increase when the–OH group points between the pair of benzene rings with ''closed'' flap angle, raising the potential energy. Conversely, the steric repulsion decreases when the–OH group points into the ''opened'' flaps, thereby lowering the potential energy for the two other minima.

This is, however, the opposite of what is observed. Our interpretation of the R2PI and fluorescence spectra of 9-hydroxytriptycene clearly shows that one of the minima is lower and two are raised in energy. This argument works for both the three minima as a function of θ for a fixed value of ϕ; and the three minima as a function of ϕ for a fixed value of θ. In both cases, there is a stabilization of one minimum over the other two. With the above arguments, this implies that the minima in the (X,Y) space correspond to an opening of the angle between benzene rings. However, this is an interpretation and *is not experimentally determined*. The data could also be interpreted as the unique minimum occurring with the–OH group between two benzene rings that is reduced from 120°. This would seem less likely on steric grounds. Even more unlikely possibilities is that the geometry at the unique minimum is with the–OH group over one benzene ring, with the opposite two rings either open or closed.

Since the common parameters between triptycene and 9-hydroxytriptycene are very similar, we conclude that geometry of these molecules at the Jahn–Teller minima is similar. While the sign of the distortion along the e_x coordinate in the S_1 state cannot be unambiguously determined from the experimental data, the present work can be interpreted in terms of a ring opening from the 120°. However, it should be noted that in this case none of the parameters or conclusions of these previous works are altered, only the sign of the e_x coordinate.

V. CONCLUSIONS

The analysis of the R2PI spectrum of 9-hydroxytriptycene indicates that the torsional motion of the–OH group interacts strongly with the Jahn–Teller active flapping motion of the benzene rings of TOH. A $E\otimes(e\oplus\phi)$ vibronic Hamiltonian was developed which, together with the parameters listed in Table II, was found to reproduce both the $S_1\leftarrow S_0$ spectrum measured by R2PI, and all the $S_1\rightarrow S_0$ fluorescence emission spectra of this molecule, in great detail. The model consists of the $E\otimes e$ Hamiltonian of unsubstituted triptycene, a threefold torsional potential for the internal rotation of the–OH group and the lowest order coupling between these coordinates. The coupling between

Jahn–Teller and–OH motions was necessary to reproduce the spectra. This coupling was also required in the ground electronic state (where this *e* flapping vibrational mode is not Jahn–Teller active) to reproduce the spectral intensities.

The sign of the coupling parameter, B_1, in the S_1 excited state implies that the geometry of the TOH molecule in the minima of the Jahn–Teller coordinate space is one where there is an *increase* in the angle between two benzene rings. This conclusion comes from steric requirements and resolves the ambiguity of the Jahn–Teller geometry in the S_1 state of triptycene.

There are two static viewpoints that can be taken. Considering the–OH group as fixed at a position midway between two benzene units results in one of the Jahn–Teller wells being lower than the other two. Alternatively, considering the triptycene molecule fixed at an e_x distortion with angle between two benzene rings opening, results in one of the minima of the torsional coordinate being lowered with respect to the other two. The transitions to vibronic levels whose wave functions are localized in the lower and upper wells appear in the spectrum and correspond to the bands $\mathbf{a_2}$ and the pair $\mathbf{e_2}$ and $\mathbf{e_3}$, respectively. The viewpoints given above are useful for visualizing the geometry of three dimensional potential energy surface, however, it would be incorrect to view the TOH molecule in its S_1 electronic state to be static with respect to either θ or ϕ coordinates.

The tunneling splitting of the lowest vibronic levels of the θ or ϕ coordinates *considered in isolation* are calculated to have similar magnitudes. However, there is only *one* calculated tunneling splitting for the lowest vibronic levels of the $E\otimes(e\oplus\phi)$ potential energy surface. Tunneling between the three lowest of the nine minima results in the concerted motion of *both* θ and ϕ coordinates. This motion follows a closed spiral path on a torus that encloses the conical intersection, leading to a sign change as required by Berry's phase. The rate at which 9-hydroxytriptycene will tunnel between minima is calculated to be much slower compared to triptycene. The Jahn–Teller pseudorotation is forced to tunnel in concert with the–OH internal rotation on the much longer time scale. The molecule may be an ideal candidate for the time-resolved detection of Berry's phase in an isolated molecule.[17]

ACKNOWLEDGMENTS

This research was supported by the Swiss National Science Foundation (Grant Nos. 20-40669.94 and 20-47214.96). We gratefully acknowledge Professor W. Adcock (Adelaide) for providing a sample of 9-hydroxytriptycene. The use of computer facilities of the High Performance Computing Unit at the University of Queensland is acknowledged.

[1] A. Furlan, M. J. Riley, and S. Leutwyler, J. Chem. Phys. **96**, 7306 (1992).
[2] A. Furlan, T. Fischer, P. Fluekiger, H. U. Güdel, S. Leutwyler, H. P. Lüthi, M. J. Riley, and J. Weber, J. Phys. Chem. **96**, 10713 (1992).
[3] A. Furlan, S. Leutwyler, and M. J. Riley, J. Chem. Phys. **100**, 840 (1994).
[4] M. J. Riley, H. U. Güdel, and A. Norton, Chem. Phys. **166**, 19 (1992).
[5] M. J. Riley, A. Furlan, H. U. Güdel, and S. Leutwyler, J. Chem. Phys. **98**, 3803 (1993).
[6] M. J. Riley and A. Furlan, Chem. Phys. **210**, 389 (1996).
[7] A. Furlan, S. Leutwyler, M. J. Riley, and W. Adcock, J. Chem. Phys. **99**, 4932 (1993).
[8] O. Cheshnovsky and S. Leutwyler, J. Chem. Phys. **88**, 4127 (1988).
[9] W. Adcock and V. S. Iyer, J. Org. Chem. **53**, 5259 (1988).
[10] E. V. Ivash and D. M. Dennison, J. Chem. Phys. **21**, 1804 (1953).
[11] F. Imashiro, K. Hirayama, T. Terao, and A. Saika, J. Am. Chem. Soc. **109**, 729 (1987).
[12] M. C. M. O'Brien, Proc. R. Soc. London, Ser. A **281**, 323 (1959).
[13] A Furlan, Ph.D. thesis, University of Berne, Switzerland.
[14] R. P. Brent, *Algorithms for Minimization Without Derivatives* (Prentice–Hall, Edgewood-Cliffs, NJ, 1973).
[15] F. S. Ham, Phys. Rev. Lett. **58**, 725 (1987).
[16] M. V. Berry, Proc. R. Soc. London, Ser. A **392**, 45 (1984).
[17] J. A. Cina and T. J. Smith, Jr., Adv. Chem. Phys. **83**, 1 (1993).